PLOS ONE

Investigation of Climate Change Impact on Water Resources for an Alpine Basin in Northern Italy: Implications for Evapotranspiration Modeling Complexity

Giovanni Ravazzani[1]*, Matteo Ghilardi[1], Thomas Mendlik[2], Andreas Gobiet[2], Chiara Corbari[1], Marco Mancini[1]

1 Politecnico di Milano, Piazza Leonardo da Vinci, Milan, Italy, 2 Wegener Center for Climate and Global Change and Institute for Geophysics, Astrophysics, and Meteorology, University of Graz, Graz, Austria

Abstract

Assessing the future effects of climate change on water availability requires an understanding of how precipitation and evapotranspiration rates will respond to changes in atmospheric forcing. Use of simplified hydrological models is required beacause of lack of meteorological forcings with the high space and time resolutions required to model hydrological processes in mountains river basins, and the necessity of reducing the computational costs. The main objective of this study was to quantify the differences between a simplified hydrological model, which uses only precipitation and temperature to compute the hydrological balance when simulating the impact of climate change, and an enhanced version of the model, which solves the energy balance to compute the actual evapotranspiration. For the meteorological forcing of future scenario, at-site bias-corrected time series based on two regional climate models were used. A quantile-based error-correction approach was used to downscale the regional climate model simulations to a point scale and to reduce its error characteristics. The study shows that a simple temperature-based approach for computing the evapotranspiration is sufficiently accurate for performing hydrological impact investigations of climate change for the Alpine river basin which was studied.

Data Availability: The authors confirm that all data underlying the findings are fully available without restriction. All relevant data are within the paper and Dataset S1. Meteorological observations can be requested to ARPA Piemonte (Contact person: Secondo Barbero secondo.barbero@arpa.piemonte.it). The relevant hydrological simulation data in the paper are raw data and not processed results.

Competing Interests: The authors have declared that no competing interests exist.

* Email: giovanni.ravazzani@polimi.it

Introduction

According to the Fifth Assessment Report (AR5) of the United Nations Intergovernmental Panel on Climate Change (IPCC) [1], for average annual Northern Hemisphere temperatures, the period 1983–2012 was very likely the warmest 30-year period of the last 800 years. Climate change has significant implications for the environment [2], [3], water resources [4], and human life in general [5], which have motivated a multitude of scientific investigations over the past two decades [6], [7], [8], [9]. One of the expected impacts of climate change is a modification of water availability, due to the strict interaction between the climate system and the hydrological cycle. Therefore, an accurate assessment of the future effects of climate change requires an understanding of how precipitation and evapotranspiration rates will respond to changes in atmospheric forcing. The most common approach used to assess the hydrologic impact of global climate change involves climate models as input of hydrological models. In particular, the climate models simulate the climatic effects of

increasing atmospheric concentrations of greenhouse gases, while the hydrological models are used to simulate the hydrological impacts of climate change [10]. River discharges, and their temporal distributions, are strongly affected by high mountainous areas [11], [12], which are particularly sensitive to global warming [13], [14]. The quality of hydrological impact investigations, even of larger catchments, thus depends on the capability to model those specific processes in mountainous regions.

The extreme complexity of the processes involved in the hydrology of mountainous areas, and the great spatial variability of meteorological forcings and river basin characteristics, require the use of physically based and spatially distributed hydrological models to simulate the transformation of rainfall into runoff [15], [16], [17]. Recent advances have made physically based hydrologic models more complex through the inclusion of more sophisticated land surface models, which compute the water and energy balances between the land surface and the atmosphere [18], [19]. This should improve the predictive skill, and facilitate the estimation of parameter values based on physiological
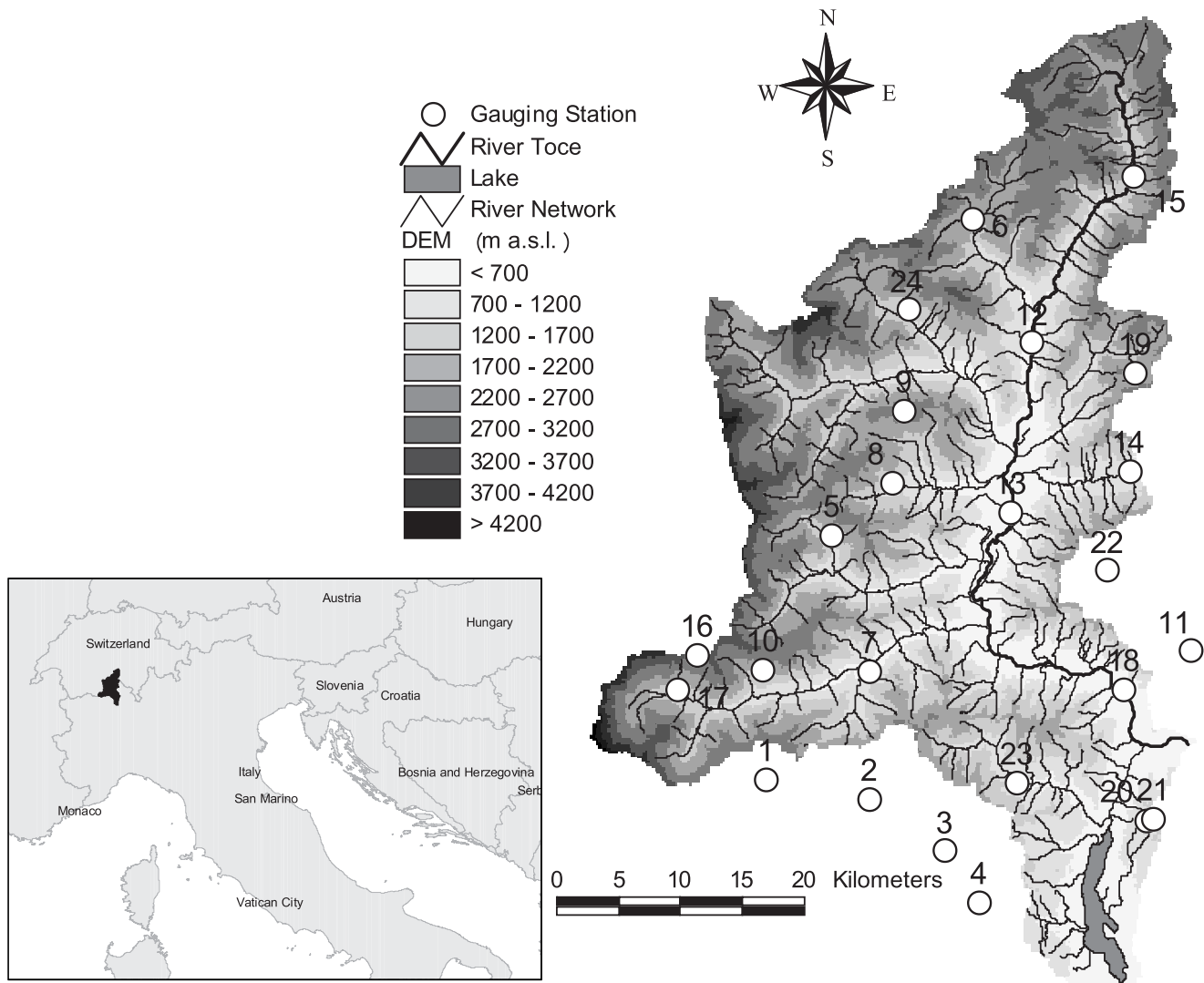
Figure 1. Localization of the stations on a DEM of the Toce watershed.
doi:10.1371/journal.pone.0109053.g001

characteristics or measurements. Conversely, more complex models suffer from computational requirements, which can limit their applicability when simulating long time series such as those required for climate change impact analyses. Moreover, in addition to precipitation and temperature data, more sophisticated models require, as an input, a complete dataset of meteorological forcings, including solar radiation, wind speed, and relative humidity. These variables may not be available, at proper spatial and temporal resolutions, to accurately capture the dynamics of the hydrological processes in mountainous areas [20]. As a consequence, the hydrological model used for the analysis of climate change impacts should be a compromise between its accuracy and its simulation time. This requires an assessment of the reliability of simplified hydrological models in contrast to the more sophisticated land surface models.

The main objective of this study was to quantify the differences between a simplified hydrological model, which computes the hydrological balance based on precipitation and temperature only, and an enhanced version of the model, which solves the energy balance to compute the actual evapotranspiration. The study was performed in three steps: first, the hydrological models were calibrated and validated against the river discharge measured in the control period; second, the hydrological models driven by climatic forcings were evaluated for their performance in reproducing the water balance components during the control period; and third, climate change impacts was assessed computing the differences between the hydrological variables simulated for the decade spanning 2041–2050 and those of the control period.

The structure of the paper is as follows. In section 2, description of the study area, and data and mathematical models used are presented. In section 3.1, the hydrological models driven by meterological forcings, are evaluated in reproducing the daily streamflow; in section 3.2 the hydrological models, driven by modelled climatic forcings, are evaluated in reproducing the hydrological aspects of the control period; in section 3.3 the climate change impacts on hydrological processes are presented. In the last section, conclusions are drawn.

Table 1. Availability of data at the stations used in the hydrological analysis.

ID	Name	Precipitation (mm)	Temperature (°C)	Radiation (w/m²)	Wind Speed (m/s)	Relative Humidity (%)	Discharge (m³/s)
1	Carcoforo		X				
2	Fobello	X	X				
3	Sabbia	X	X				
4	Varallo	X	X			X	
5	Alpe Cheggio		X				
6	Alpe Devero	X	X			X	
7	Anzino	X	X				
8	Pizzanco	X	X			X	
9	Lago Paione	X	X	X		X	
10	Ceppo Morelli		X				
11	Cicogna	X	X				
12	Crodo	X	X			X	
13	Domodossola	X	X	X	X	X	
14	Druogno	X	X			X	
15	Formazza	X	X			X	
16	Passo Moro	X	X			X	
17	Pecetto	X	X				
18	Candoglia	X	X				X
19	Larecchio	X	X			X	
20	Baita CAI	X	X				
21	Mottarone	X	X			X	
22	Mottac	X	X				
23	Sambughetto	X	X				
24	Varzo	X	X			X	

Data and Methods

Study area

The Toce watershed is a typical glacial basin, with steep hillslopes bounding a narrow valley located primarily in the north Piedmont region of Italy, and partially in Switzerland (10% of the total area), and with a total drainage area of approximately 1,800 km² (Fig. 1). Its elevation ranges from 193 m above sea level (a.s.l.) at the outlet to approximately 4,600 m a.s.l. at the Monte Rosa crest. The average elevation is 1,641 m a.s.l. Geographic coordinates of basin outlet are: 8.49027° longitude, 45.94028° latitude.

The land cover is composed of forests (70%), bare rocks (9%), agricultural land (7%), natural grassland (6%), urban centers (4%), bodies of water (3%), and glaciers and perpetual snow (1%). The Toce lithology has five main classes: augean gneiss (49%), micaceous schists (27%), calcareous schists (11%), grindstones (7%), and granites (6%). The steep hillslopes, forming the most significant area of the basin, are mostly covered by trees on thin soil layers resting on bedrock. The soil depth increases in the downstream narrow alluvial region where an unconfined aquifer interacts with the river course. Fourteen major dams are located within the Toce watershed, with a total effective storage capacity of approximately 151×10⁶ m³ [21].

A digital elevation model was available at a 200×200 meter resolution as retrieved from 1:10,000-scale topographic maps [22]. The digital land use map was derived by coupling the CORINE (Coordination of Information on the Environment) land cover map [23] for the Italian portion, with the Swiss land use map (Arealstatistik) for the small portion of the basin located in Switzerland. Both the maps were derived from remote sensing observations [21]. Most of the parameter maps were produced during the European Union research project RAPHAEL (Runoff and Atmospheric Processes for flood HAzard forEcasting and controL), whose objective was to improve flood forecasting in the complex mountain watershed [24], [25].

The meteorological and hydrologic data were collected hourly by a telemetric monitoring system of the Regione Piemonte flood warning system. The data were available from January 1, 2000 to December 31, 2010 at the stations shown in Table 1 and Fig. 1 for the rainfall, air temperature, short wave solar radiation, air humidity, wind speed, and river discharges at Candoglia (1,534 km² basin area). The mean value of the maximum annual flood peak is 944 m³/s, and the average discharge is 64 m³/s.

Two hydrological models with increasing complexity

Two distributed hydrological models were used for simulating the water balance components of the Toce river basin: the FEST-WB (Flash–flood Event–based Spatially distributed rainfall–runoff Transformation, including Water Balance [15], [26]) and the FEST-EWB (Flash–flood Event–based Spatially distributed rainfall–runoff Transformation, including Energy and Water Balance [27], [18]). The main difference between them is in the computation of evapotranspiration. The FEST-WB model derives the actual evapotranspiration by rescaling the potential evapotranspiration using a simple empirical approximation, where the

Table 2. Meteorological forcings and parameters used as input to the FEST-WB and FEST-EWB models.

Input	Unit	FEST-WB	FEST-EWB
Precipitation	mm	X	X
Temperature	°C	X	X
Solar Radiation	W/m^2		X
Wind Speed	m/s		X
Relative Humidity	%		X
Saturated Hydraulic Conductivity	m/s	X	X
Residual Moisture Content	-	X	X
Saturated Moisture Content	-	X	X
Wilting Point	-	X	X
Field Capacity	-	X	X
Pore Size Index	-	X	X
Curve Number	-	X	X
Soil Depth	m	X	X
Vegetation Fraction	%	X	X
Crop Coefficient	-	X	
Leaf Area Index	m^2/m^2		X
Albedo	-		X
Minimum Stomatal Resistance	s/m		X
Vegetation Height	m		X

doi:10.1371/journal.pone.0109053.t002

potential evapotranspiration is computed based only on air temperature measurements. By contrast, the FEST-EWB model computes the actual evapotranspiration by solving the system of water mass and energy balance equations. The differences in the input parameters and meteorological forcings are listed in Table 2.

Six principal components can be identified in all models (Fig. 2): 1) the flow paths and channel network definition; 2) the spatial interpolation of meteorological forcings; 3) the simulation of snow pack and glacier dynamics; 4) the estimation of losses and soil moisture updating; 5) the runoff and base flow routings, including the effect of artificial reservoirs; and 6) the groundwater and hyporheic exchanges with streamflow.

For further details on distributed hydrological models and their applications, the reader can refer to [28], [29], [30], [31], [32], [33], [34].

Actual evapotranspiration in the FEST-WB hydrological model. The global actual evapotranspiration rate is given by:

$$ET = f_{bs}E_{bs} + f_v T \qquad (1)$$

where E_{bs} is the actual rate of bare soil evaporation, T is the actual rate of transpiration, and f_{bs} and f_v are the fraction of the bare soil and the vegetation area, respectively ($f_{bs} + f_v = 1$). The actual rates of the bare soil evaporation and transpiration are computed as a fraction of the potential evapotranspiration, PET:

$$E_{bs} = \alpha(\theta) PET \qquad (2a)$$

$$T = \beta(\theta) PET \qquad (2b)$$

where

$$\alpha(\theta) = 0.082\theta + 9.173\theta^2 - 9.815\theta^3 \qquad (3a)$$

$$\beta(\theta) = \begin{cases} 0 & if \quad \theta \leq \theta_{wp} \\ 1 & if \quad \theta \geq \theta_{fc} \\ \dfrac{\theta - \theta_{wp}}{\theta_{fc} - \theta_{wp}} & if \quad \theta_{wp} < \theta < \theta_{fc} \end{cases} \qquad (3b)$$

and where θ (-), θ_{fc} (-), and θ_{wp} (-) are current water content, field capacity, and wilting point, respectively.

The potential evapotranspiration is given by

$$PET = K_c PET_0 \qquad (4)$$

where K_c is the crop coefficient [35] retrieved from satellite images [36], [37], and PET_0 is the reference potential evapotranspiration that is computed with a temperature-based equation specifically developed for the Alpine environment [38]:

$$PET = K_c PET_0$$

$$PET_0 = (0.817 + 0.00022 \cdot z) \cdot HC \cdot$$
$$R_a \cdot (T_{max} - T_{min})^{HE} \left(\frac{T_{max} - T_{min}}{2} + HT \right) \qquad (5)$$

where z is the elevation (m a.s.l.), R_a is the extraterrestrial radiation (mm·day^{-1}), T_{max} is the daily maximum air temperature
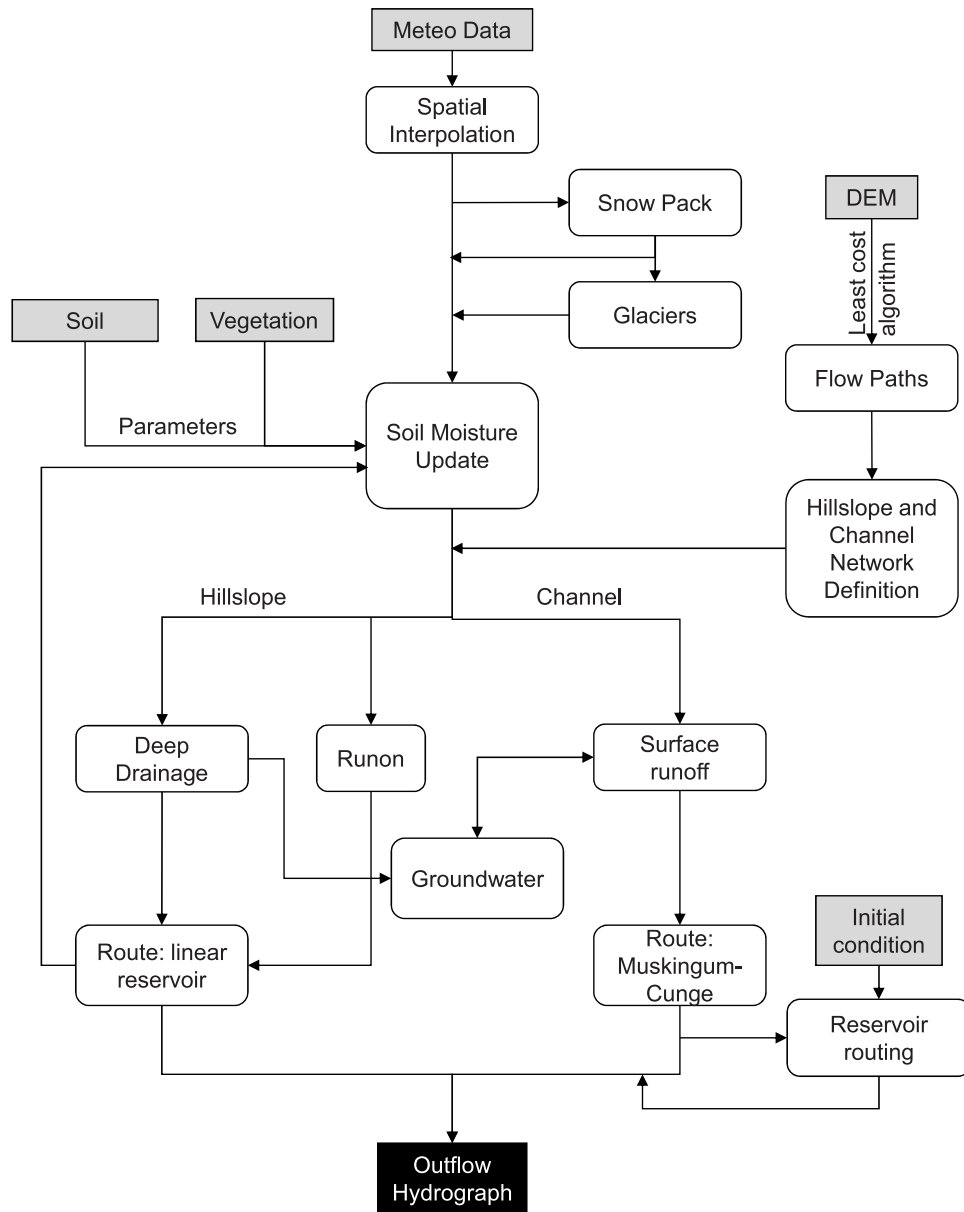
Figure 2. Scheme of the primary features common to the FEST-WB and FEST-EWB distributed-hydrological models.
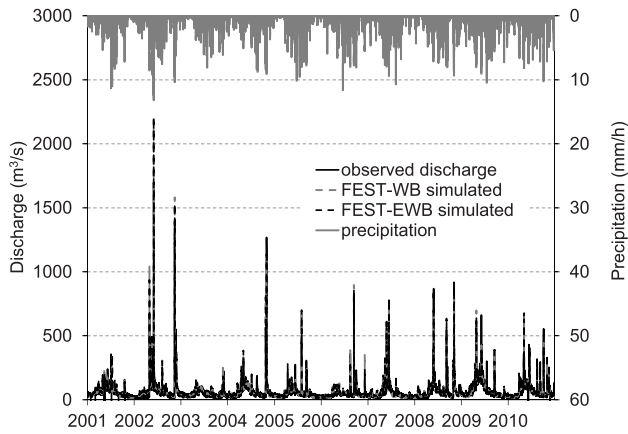doi:10.1371/journal.pone.0109053.g002

($^\circ$C), T_{min} is the daily minimum air temperature ($^\circ$C), HC is the empirical coefficient ($HC = 0.0023$), HE is the empirical exponent ($HE = 0.5$), and HT is to convert units of Fahrenheit to Celsius ($HT = 32/1.8 = 17.8$) [39].

Actual evapotranspiration in FEST-EWB hydrological model. In the FEST-EWB model, the actual evapotranspiration is computed by solving the energy balance equation at the ground surface expressed as

Table 3. Root mean square error (*RMSE*), m³/s, and Nash and Sutcliffe efficiency (η) for the FEST-WB and FEST-EWB driven by observed meteorological forcings.

Index	FEST-WB	FEST-EWB
RMSE	26.7	29.5
η	0.81	0.76

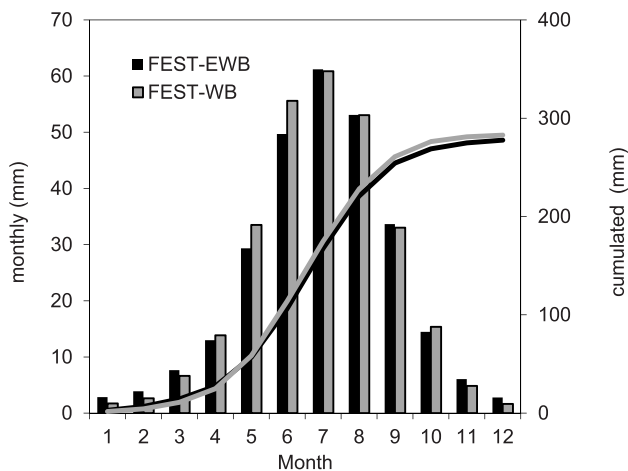doi:10.1371/journal.pone.0109053.t003

Figure 3. Comparison between the simulated and observed hourly discharge from the FEST-WB and FEST-EWB hydrological models.
doi:10.1371/journal.pone.0109053.g003

$$R_n - G - (H_S + H_C) - (LE_S + LE_C) = \frac{\Delta W}{\Delta t} \qquad (6)$$

where R_n (W·m^{-2}) is the net radiation, G (W·m^{-2}) is the soil heat flux, H_s and H_c (W·m^{-2}) and LE_s and LE_c (W·m^{-2}) are the sensible heat and latent heat fluxes for the bare soil (s) and canopy (c), respectively, and $\Delta W/\Delta t$ (W·m^{-2}) assembles the energy storage terms. These terms are often negligible, especially with a low spatial resolution at the basin scale; however, the contribution of these terms can be significant at the local scale [40], [41]. LE_c is a function of the canopy resistance, which is expressed as a function of the leaf area index, while LE_s is a function of the soil resistance [18]. In this study leaf area index was retrieved from satellite images.

All of the terms of the energy balance depend on the land surface temperature (LST), which allows the energy balance equation to be solved by finding the thermodynamic equilibrium temperature which closes the equation using the Newton-Raphson method:

Figure 4. Mean monthly and cumulated actual evapotranspiration as computed by the FEST-WB and FEST-EWB hydrological models driven by meteorological observations.
doi:10.1371/journal.pone.0109053.g004
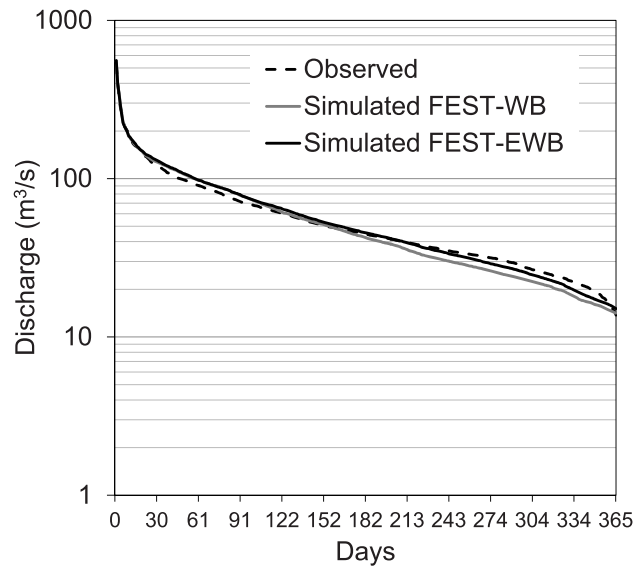
Figure 5. Mean flow duration curves for 2001–2010 from the observed discharges and those simulated by the FEST-WB and FEST-EWB hydrological models driven by meteorological observations.
doi:10.1371/journal.pone.0109053.g005

$$LST_n = LST_{n-1} + \frac{f_t(LST_{n-1})}{f_t'(LST_{n-1})} \qquad (7)$$

where LST_n is the actual value, LST_{n-1} is the value at the previous iteration, $f_t(LST_{n-1})$ is the energy balance function, and $f_t'(LST_{n-1})$ is its derivative. The solution is acceptable when $\left| \frac{f_t(LST)}{f_t'(LST)} \right| < tolerance$ and $f_t(LST) < tolerance$, with $tolerance$ equal to 0.001.

The FEST-EWB model has been proven to make accurate projections of the actual evapotranspiration against the energy and mass exchange measurements acquired by an eddy covariance station [18] and at the agricultural district scale against ground and remote sensing information [27].

Calibration and validation of the hydrological models

The calibration of the snow module parameters was performed in a previous study described by [42] and [43]. Given that the first assigned values (based upon measured values or reference literature or an educated guess) provided satisfactory results in terms of time series discharge simulation, no other parameters were calibrated. The performance of the model was assessed by comparing the daily simulated and observed discharge at Candoglia in the period from 2001 to 2010. The year 2000 was treated as the period for the model initialization. The performance of the models was assessed through two goodness of fit indices, the Root Mean Square Error (RMSE) and the Nash and Sutcliffe [44] efficiency (η), defined as follows:

$$RMSE = \left[\frac{\sum_{i=1}^{n} \left(Q_{sim}^i - Q_{obs}^i \right)^2}{n} \right]^{0.5} \qquad (8)$$

Table 4. Daily mean (*T*), maximum (*T_max*) and minimum (*T_max*) temperature and mean annual precipitation (*P*) observed and simulated by error corrected REMO and RegCM3 climate models for control period (2001–2010).

	T (°C)	*T_max* (°C)	*T_min* (°C)	*P* (mm)
observed	4.17	8.14	0.52	1412.75
REMO	4.06	8.33	0.46	1399.25
RegCM3	4.09	7.04	1.33	1339.04

doi:10.1371/journal.pone.0109053.t004

$$\eta = 1 - \frac{\sum_{i=1}^{n}\left(Q_{sim}^{i} - Q_{obs}^{i}\right)^2}{\sum_{i=1}^{n}\left(Q_{obs}^{i} - \overline{Q_{obs}}\right)^2} \qquad (9)$$

where n is the total number of time steps, Q_{sim}^{i} is the ith simulated discharge, Q_{obs}^{i} is the ith observed discharge, and $\overline{Q_{obs}}$ is the mean of the observed discharges.

## At-site bias-corrected climate-scenario forcings

For the meteorological forcing of future scenarios, two different regional climate models (RCMs) were used, the REMO [45] and the RegCM3 [46]. Both models cover Europe on a 25×25 km grid, in the same simulation period (1951–2100). Moreover, they are driven by the same global ocean-atmosphere-coupled model, ECHAM5 [47], using the observed greenhouse gas concentrations between 1951 and 2000 and IPCC's (Intergovernmental Panel on Climate Change) greenhouse gas emission scenario A1B [48] between 2001 and 2100. Both were produced within the EU FP6 Integrated Project ENSEMBLES (http://www.ensembles-eu.org/) and can be downloaded from http://ensemblesrt3.dmi.dk on a daily basis. Hourly and 3-hourly data were provided directly by the Max Planck Institute for Meteorology and the Abdus Salam International Center for Theoretical Physics. In comparison to the larger ensemble of regional simulations for Europe, the REMO and RegCM3 models represent moderate warming (below average) and near-average precipitation changes [49].
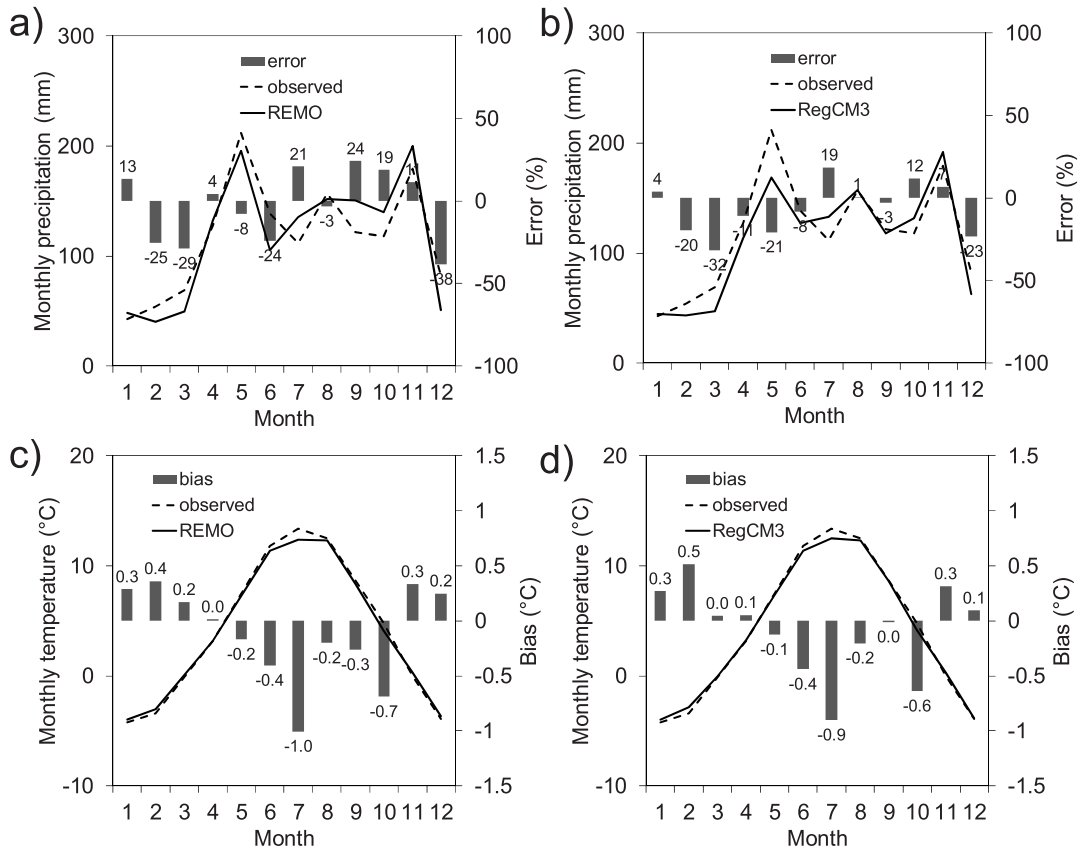
Figure 6. Mean monthly precipitation and temperature for 2001–2010 as simulated by the REMO and RegCM3 regional climate models and their deviations versus the observations.
doi:10.1371/journal.pone.0109053.g006
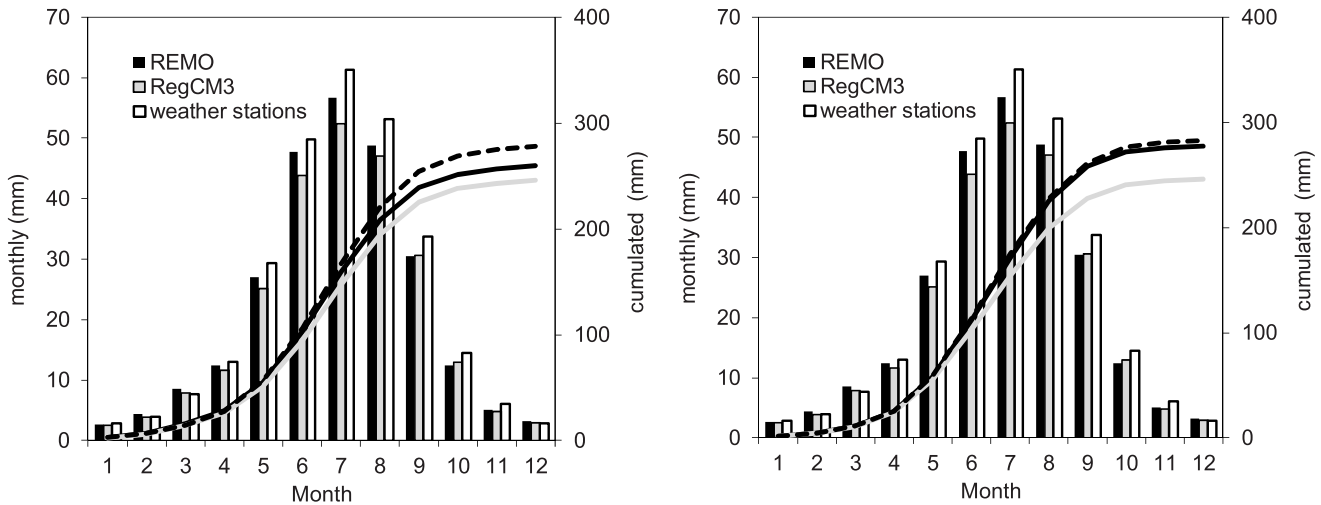
Figure 7. Mean monthly and cumulated actual evapotranspiration as computed for 2001–2010 by the FEST-EWB (left) and FEST-WB (right) hydrological models driven by the REMO and RegCM3 regional climate models and the weather observations during the control period (2001–2010).
doi:10.1371/journal.pone.0109053.g007

A quantile-based error-correction approach (quantile mapping) has been used to downscale the RCM simulations to a point scale and to reduce its error characteristics. The potential of quantile mapping for correcting GCM data has already been demonstrated in previous hydrological studies [50], [51], but its application to regional climate simulations is somewhat recent [52], [53], [54], [55], [56], [57]. In this study, the quantile mapping applied observational stations data to climate data, from the regional climate models, on a daily basis. It adapted the modelled time series to the observed empirical cumulative frequency distribution [58]. The method and its application were discussed by [59] and [54] as to what concerns daily temperature and precipitation, and by [60] as regards other meteorological variables such as relative humidity, global radiation, and wind speed. All the variables used in this study were error corrected and downscaled to a station

basis. A 31-day moving window in the calibration period, centered on the day to be corrected, was used for constructing the empirical cumulative frequency distribution for that particular day of the year. This enabled an annual cycle-sensitive correction as well as a sufficiently large sample size. A point-wise implementation, which fits a separate statistical model for each observational station, was chosen to account for the regionally varying errors. Grid cell averages (3×3) of the raw RCM data were used as predictors with respect to the effective resolution of the RCM, which is below the grid-resolution.

The calibration period for the error correction ranged from 01-01-2000 to 12-31-2009. No error correction was performed for stations with less than 9 years of observational data ($>10\%$ missing data), because the climate variability could not be expected to be properly covered by only a few years of data. Quantile mapping
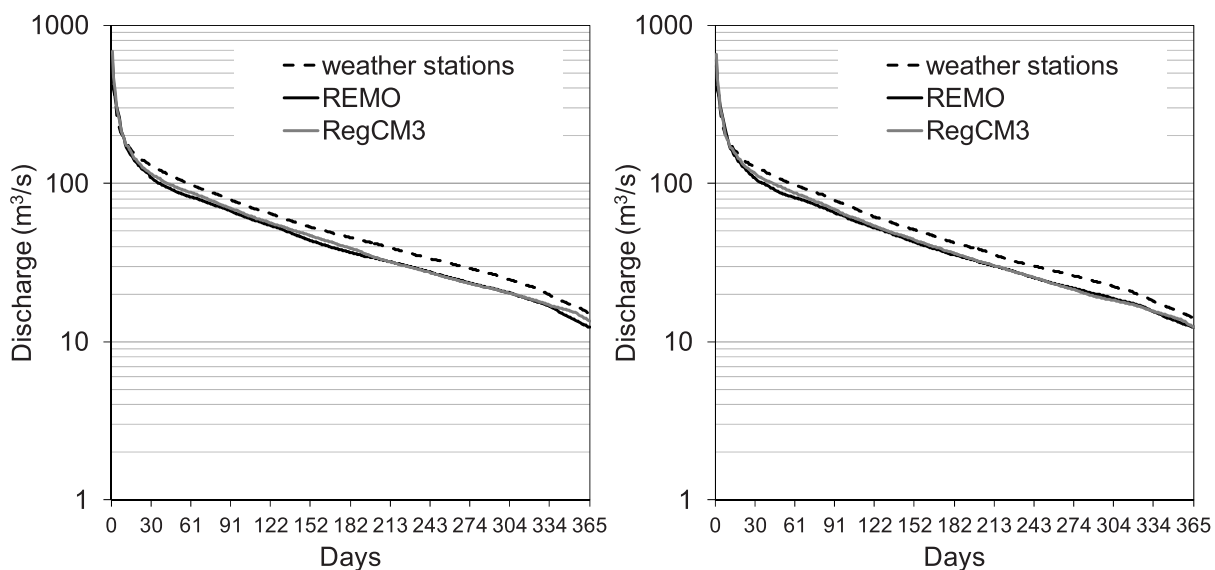
Figure 8. Mean flow duration curves simulated by the FEST-EWB (left) and FEST-WB (right) hydrological models driven by meteorological observations and the simulated climatic forcings by the REMO and RegCM3 regional climate models.
doi:10.1371/journal.pone.0109053.g008

Table 5. Daily mean (T), maximum (T_{max}) and minimum (T_{max}) temperature and mean annual precipitation (P) simulated by REMO and RegCM3 climate models for decade 2041–2050.

	T (°C)	T_{max} (°C)	T_{min} (°C)	P (mm)
REMO	5.35	9.01	1.34	1678.54
RegCM3	5.21	7.88	2.16	1578.85

assumes that the same statistical relations of the observed and modelled climate hold within the calibration period, as well as in future scenario periods. It must be kept in mind that even a calibration period of 9–10 years can be affected by decadal climate variability, which can degrade the results of the error correction applied to the future scenario period.

The resulting daily scenarios were further refined to a 3-hourly time series using the sub-daily data from the RCMs. For the air temperature, the differences between the 3-hourly RCM data and their daily-mean values were added to the corresponding corrected-daily values. The ratios of the 3-hourly RCM data and daily precipitation values were multiplied by the corrected daily values. Similarly, for the global radiation, the wind speed, and the relative humidity, the ratios of the 3-hourly RCM data and their daily mean values were multiplied by the corrected daily value. In the case of relative humidity values exceeding 100%, all

of the values from the day were multiplied by a factor to shrink the daily maximum value to 100%.

Climate-scenario dataset used in this analysis is included as supplemental file (Dataset S1).

Results and Discussion

Comparison of the models driven by meteorological observations

Table 3 shows the results in reproducing the daily streamflow by the FEST-WB and FEST-EWB models forced by meteorological observations. The goodness of fit indices of the two models are comparable, with the FEST-WB model displaying a slightly greater Nash and Sutcliffe efficiency and lower RMSE. In Fig. 3, a comparison between the FEST-WB and FEST-EWB models for the simulated and observed hourly discharge is shown for the
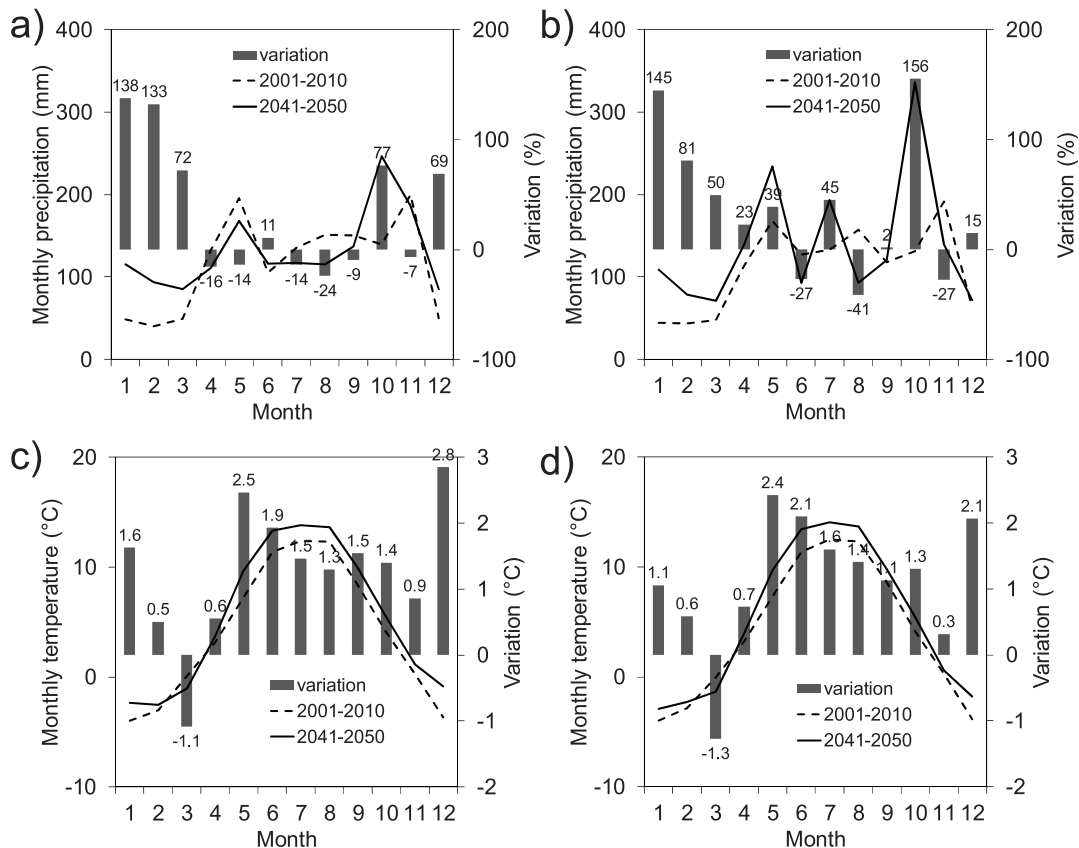
Figure 9. Mean monthly precipitation and temperature for the period 2041–2050 as projected by REMO and RegCM3 regional climate models versus the control period (2001–2010): (a) precipitation by REMO; (b) precipitation by RegCM3; (c) temperature by REMO; and (d) temperature by RegCM3.
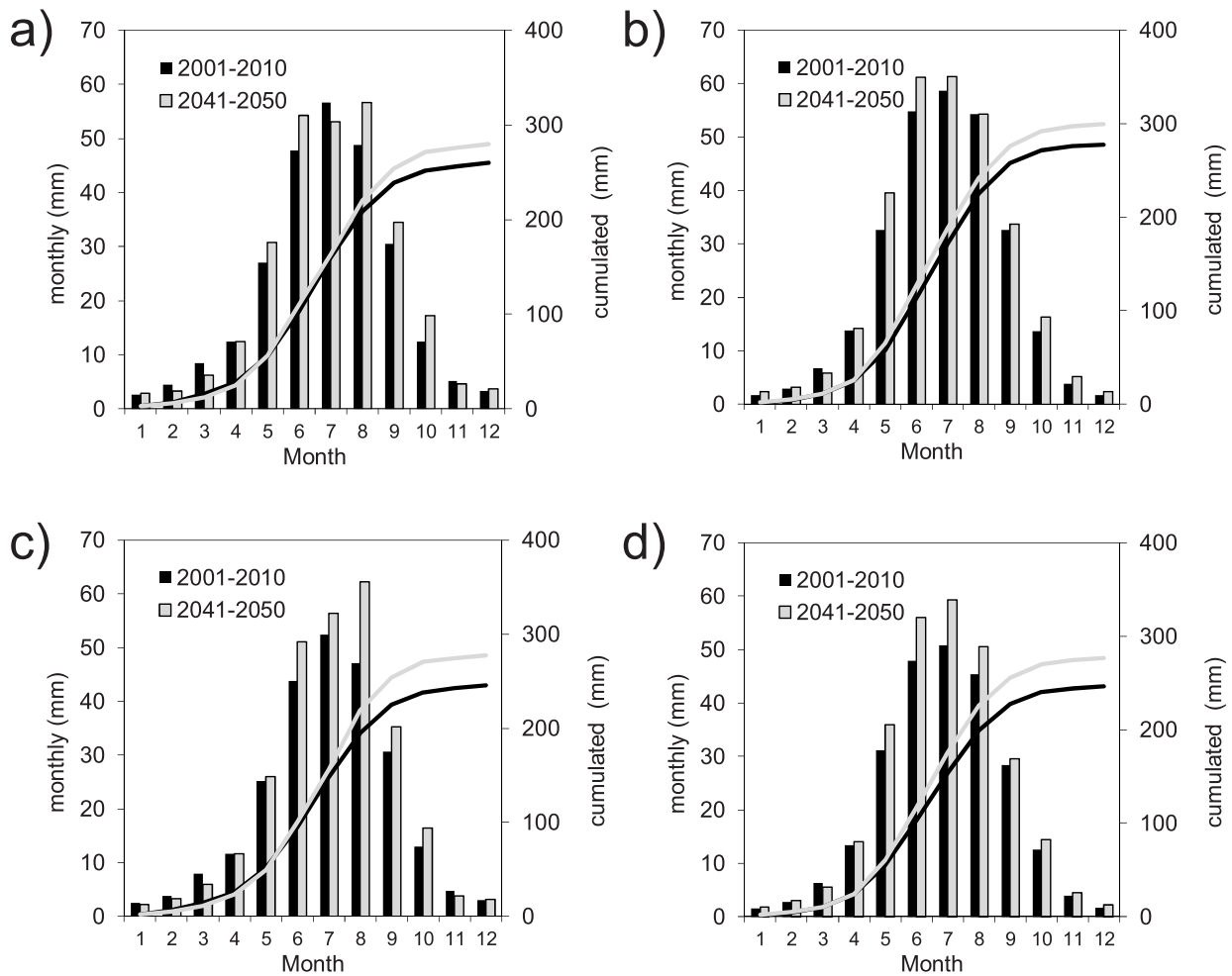
Figure 10. Mean monthly and cumulated actual evapotranspiration for the period 2041–2050 as simulated by the FEST-WB and FEST-EWB hydrological models driven by the REMO or RegCM3 regional climate models versus the control period (2001–2010): (a) FEST-EWB driven by REMO; (b) FEST-WB driven by REMO; (c) FEST-EWB driven by RegCM3; and (d) FEST WB driven by RegCM3.
doi:10.1371/journal.pone.0109053.g010

period from 2001 to 2010. The differences were almost negligible and the time series overlapped.

The mean monthly and cumulated actual evapotranspiration values, as computed by the FEST-WB and FEST-EWB models driven by meteorological observations, are shown in Fig. 4. There is a general agreement between the two different approaches in computing the evapotranspiration with the exceptions of May and June, when the FEST-WB model had values 14% and 12% higher, respectively, than the FEST-EWB model. On an annual basis, the FEST-WB model had a 1.8% higher value than the FEST-EWB model.

In Fig. 5, the mean flow duration curves simulated by the two models are compared to those observed. Good agreement was seen for both the higher and lower discharges. The difference between the FEST-WB and FEST-EWB simulations was due to the different evapotranspiration losses reported by the two models.

Comparison of models in reproducing the hydrological aspects of the control period

Before assessing the climate change impacts, we performed an analysis of the hydrological models, driven by modelled climatic forcings, in reproducing the hydrological aspects of the control period (2001–2010). Table 4 shows the mean annual precipitation

and the average daily mean, maximum, and minimum temperatures observed and simulated by the calibrated REMO and RegCM3 climate models during the control period. The REMO model resulted in a $0.11°C$ and 0.95% underestimation in reproducing the temperature and precipitation, respectively, while the RegCM3 model resulted in a $0.08°C$ and 5.2% underestimation.

The two climate models displayed larger differences in reproducing the daily maximum and minimum temperature. The REMO model produced errors of $0.2°C$ and $-0.1°C$ in reproducing the maximum and minimum daily temperatures, respectively, while the RegCM3 model produced errors of $-1.1°C$ and $0.8°C$, respectively. This can be explained by the fact that only the daily mean values were error corrected, while the diurnal cycle was superimposed as the models simulated it without further correction (Section 2.4).

In Fig. 6, the mean monthly precipitation and temperature, as simulated by the REMO and RegCM3 climate models, are compared to those observed. Regarding precipitation, the two models underestimated it in February, March, May, June, and December and overestimated it in July, October, and November. Nevertheless, the overall behavior, such as the peaks in the spring and autumn, was well captured. The two climatic models
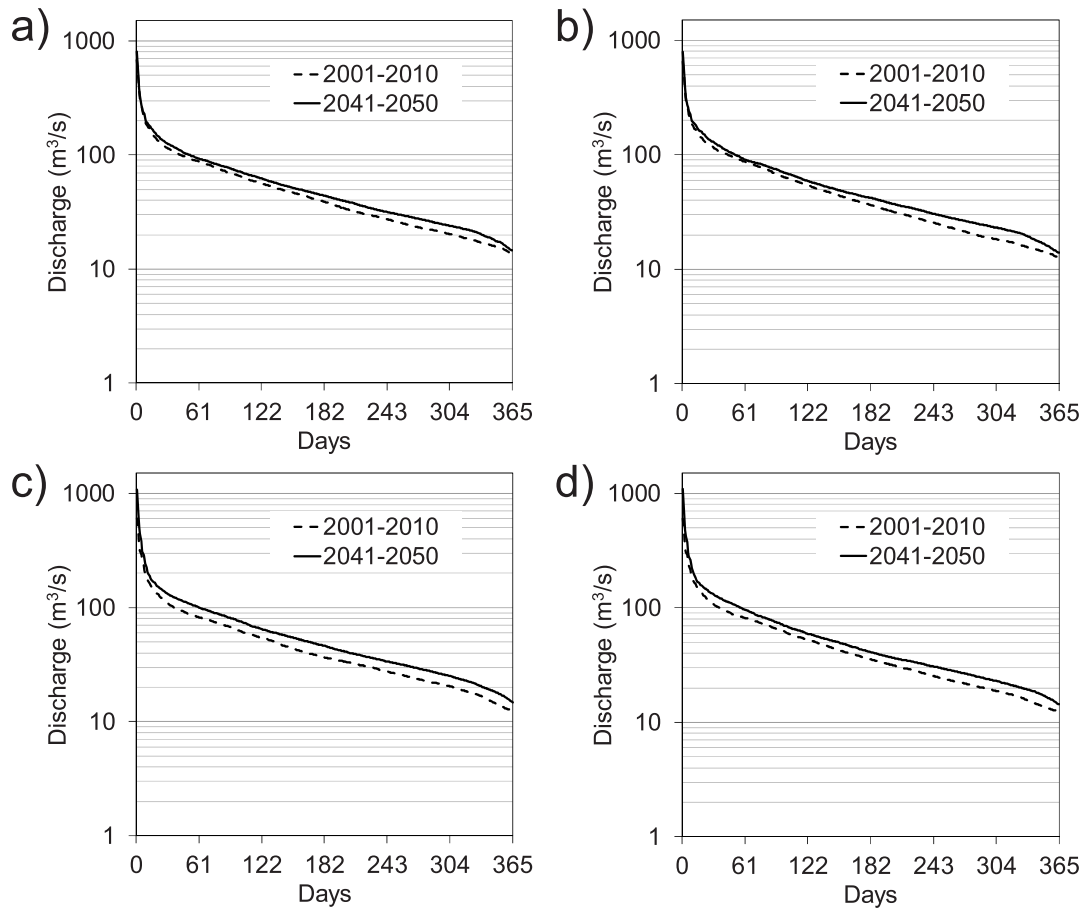
Figure 11. Mean flow duration curve for the period 2041–2050 as simulated by the FEST-WB and FEST-EWB hydrological models driven by the REMO or RegCM3 regional climate models versus the control period (2001–2010): a) FEST-EWB driven by REMO, b) FEST-WB driven by REMO, c) FEST-EWB driven by RegCM3, and d) FEST WB driven by RegCM3.
doi:10.1371/journal.pone.0109053.g011

displayed the same results in reproducing the monthly temperatures, that is, they underestimated it from May to October and overestimated it in the other months of the year, but the discrepancies were under the acceptable limits.

Since the evaluation period differs from the calibration period of the bias correction, such minor discrepancies should be expected. An increase of these errors in future applications should also be expected. However, this increase can be regarded as limited, given that the bias correction is relatively stable, as has been demonstrated by [61] and [60].

Fig. 7 shows the mean monthly and cumulated actual evapotranspiration as computed by the FEST-EWB and FEST-WB hydrological models driven by REMO, RegCM3, and meteorological observations during the control period. Both the FEST-EWB and FEST-WB models simulated greater evapotranspiration when driven by REMO than by RegCM3. The FEST-WB equation to compute the evapotranspiration is very sensible to the daily temperature range. This implies that the evapotranspiration computed by the FEST-WB model, driven by REMO, matches the evapotranspiration computed by the FEST-WB model, driven by the meteorological observations, as the REMO model is more accurate than the RegCM3 model in reproducing the daily minimum and maximum temperatures.

Fig. 8 shows the mean flow duration curves simulated by the FEST-EWB and FEST-WB hydrological models driven by

meteorological observations and the REMO and RegCM3 simulated climatic forcings. There was good agreement between the REMO and RegCM3 driven simulations. The discharges driven by the RegCM3 model were generally greater than those driven by REMO, particularly for the high durations, due to the underestimation of the evapotranspiration component.

Projected changes in the hydrological processes

The impacts of climate change on hydrological processes were assessed by comparing the results from the FEST-EWB and FEST-WB models, driven by the REMO and RegCM3 climate models, for the decade spanning 2041–2050 to those of the control period. The simulations were performed assuming no variation in the spatial distribution of the vegetation, or the beginning and duration of the growing season. This means that the crop coefficient functions for the future period were unmodified, and that the monthly leaf area index maps were derived as an average from the 2001–2010 remotely sensed maps.

Table 5 shows the average daily mean, maximum, and minimum temperatures and the mean annual precipitation simulated by the REMO and RegCM3 models for the 2041–2050 decade. The REMO and RegCM3 models simulated an increase in mean temperature of 1.28°C and 1.12°C, respectively, and an increase in the mean annual precipitation of 12.83% and 25.35%, respectively.
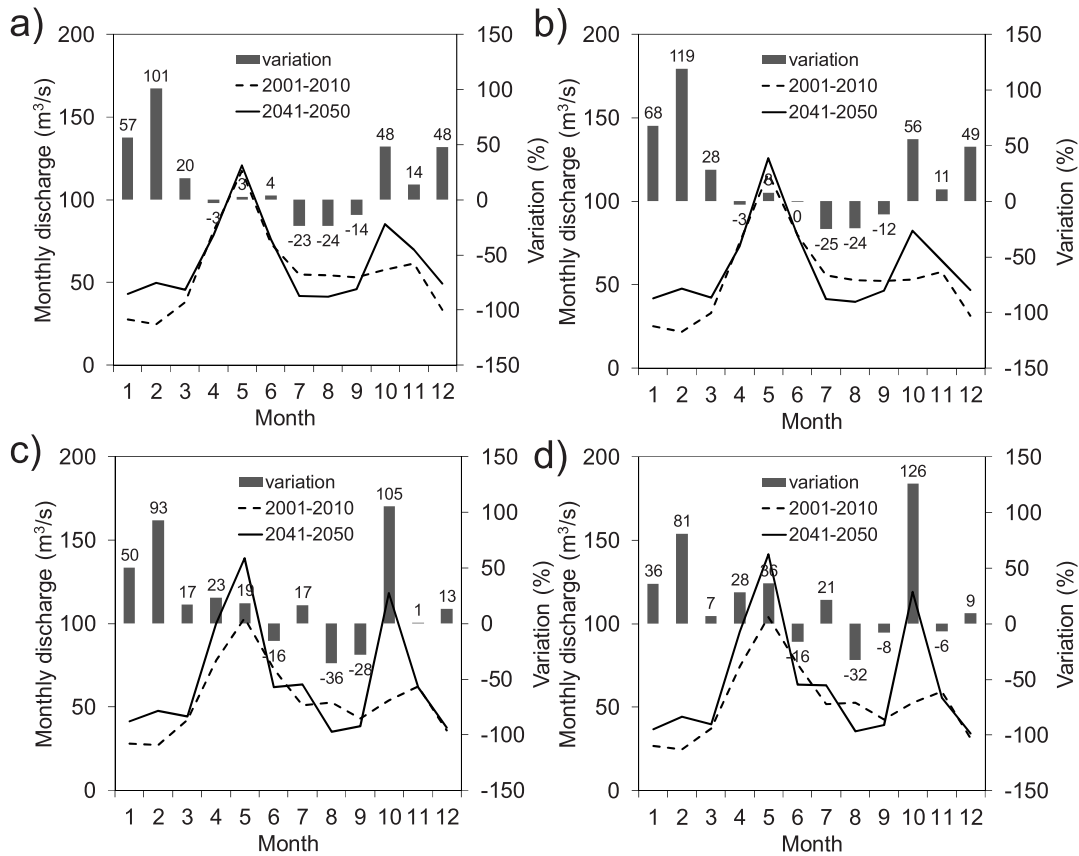
Figure 12. Mean monthly discharge for the period 2041–2050 as simulated by the FEST-WB and FEST-EWB hydrological models driven by the REMO or RegCM3 regional climate models versus the control period (2001–2010): a) FEST-EWB driven by REMO, b) FEST-WB driven by REMO, c) FEST-EWB driven by RegCM3, and d) FEST WB driven by RegCM3.
doi:10.1371/journal.pone.0109053.g012

The mean monthly precipitation and temperature as simulated by REMO and RegCM3 for the control period (2001–2010) and for the 2041–2050 decade are shown in Fig. 9. The precipitation increase was mostly concentrated in the winter period and October, in which the RegCM3 model projected a precipitation increase of 156%. During the summer, the two climate models projected a significant decrease in precipitation, as much as −41% in August by the RegCM3 model. The temperature was generally predicted to increase more significantly during the summer, late spring, and winter, while a decrease was expected in March. These results are consistent with findings depicted in the IPCC AR4 for Central Europe [62] and with a recent review on expected climate change in the Alpine region [14].

Fig. 10 shows the mean monthly and cumulated actual evapotranspiration as computed by the FEST-EWB and FEST-WB models driven by REMO and RegCM3 for the control period (2001–2010) and the 2041–2050 decade. All of the simulations showed an increase in the evapotranspiration, in agreement with the increase in air temperature. For a given climate model, the FEST-EWB and FEST-WB hydrological models projected similar modifications to the evapotranspiration.

In Fig. 11, the mean flow duration curves simulated by the FEST-EWB and FEST-WB hydrological models, driven by REMO and RegCM3 for the 2041–2050 decade, were compared to those of the control period (2001–2010). A general increase of the discharge was projected for the flow duration, in agreement with the significantly increased annual precipitation not compen-

sated by increased evapotranspiration. For a given climate model the FEST-EWB and FEST-WB hydrological models predicted similar modifications to the flow duration curve.

In Fig. 12, the mean monthly discharge for the 2041–2050 decade, simulated by the FEST-EWB and FEST-WB hydrological models driven by the REMO and RegCM3 climate models, is compared to that of the control period (2001–2010). The seasonal shift observed in the precipitation was reflected in the projected monthly discharge, with a significant increase expected in October and in the winter period and a significant decrease expected in summer.

Conclusions

This study investigated the role of climatic forcing availability, and thus hydrological model complexity, on the assessment of climate change impacts on the water resources for the Toce river basin. Two distributed hydrological models were used to simulate the water balance components of the Toce river basin: the FEST-WB model, which implements a simple temperature-based method for computing the evapotranspiration; and the FEST-EWB model, which computes evapotranspiration by solving energy and water balance equations that require temperature, net radiation, wind speed, and relative air humidity as meteorological forcings. Both the FEST-WB and FEST-EWB models performed well in reproducing the daily discharge of the 2001–2010 period and the hourly discharge for major flood events. The difference in computing the evapotranspiration was approximately

2% on an annual basis. Moreover, there was general agreement between the two hydrological models in reproducing the mean annual flow-duration curve.

An analysis of the hydrological models, driven by the climatic forcings modelled by the REMO and RegCM3 climate models, in reproducing the hydrological aspects of the control period showed that the FEST-WB model was more sensitive to the daily temperature range in simulating the evapotranspiration. The evapotranspiration differences impacted the flow duration curve, but the two hydrological models achieved good agreement.

The impact of climate change on the hydrological processes was assessed by comparing the results from the FEST-EWB and FEST-WB models, driven by REMO and RegCM3 for the 2041–2050 decade, to those of the control period (2001–2010). The REMO and RegCM3 climate models simulated increased mean temperatures, and increased mean annual precipitations. The precipitation increase was primarily concentrated during October and the winter period. The two climate models predicted a significant decrease in precipitation during the summer. This reflects an increase in the evapotranspiration and the discharges for all of the durations in the flow duration curves. The seasonal shift observed in the precipitation was reflected in the monthly discharge. Indeed, a significant increase in the discharge was expected in October and the winter period, while a significant decrease was expected in the summer. Obtained results are generally consistent with findings depicted in the IPCC assessment reports.

In general, this study showed that despite the simple temperature-based approach for computing evapotranspiration, the FEST-WB model is robust and sufficiently accurate to perform hydrological impact studies of climate change for the Alpine river basin that was investigated. The bias introduced by the approximations from the method used to compute the evapotranspiration was less than the uncertainty associated with climate models.

Supporting Information

Dataset S1 At-site bias-corrected climate data used in the hydrological models for the period 1951–2050, which include 3-hourly data for rainfall in mm (PRE_3hc.txt), air temperature in °C (TAS_3hi.txt), wind speed in m/s (WSS_3hi.txt), solar radiation in W/m^2 (RSDS_3hi.txt), and percentage relative humidity (HURS_3hi.txt).
(ZIP)

Acknowledgments

Author Contributions

References

1. IPCC (2013) Climate Change 2013: The Physical Science Basis. Contribution of Working Group I to the Fifth Assessment Report of the Intergovernmental Panel on Climate Change [Stocker, T.F., D. Qin, G.-K. Plattner, M. Tignor, S.K. Allen, J. Boschung, A. Nauels, Y. Xia, V. Bex and P.M. Midgley (eds.)]. Cambridge University Press, Cambridge, United Kingdom and New York, NY, USA, 1535 pp.

2. Loarie SR, Carter BE, Hayhoe K, McMahon S, Moe R, et al. (2008) Climate Change and the Future of California's Endemic Flora. PLoS ONE 3(6): e2502. doi:10.1371/journal.pone.0002502.

3. Shrestha UB, Gautam S, Bawa KS (2012) Widespread Climate Change in the Himalayas and Associated Changes in Local Ecosystems. PLoS ONE 7(5): e36741. doi:10.1371/journal.pone.0036741.

4. Dile YT, Berndtsson R, Setegn SG (2013) Hydrological Response to Climate Change for Gilgel Abay River, in the Lake Tana Basin - Upper Blue Nile Basin of Ethiopia. PLoS ONE 8(10): e79296. doi:10.1371/journal.pone.0079296.

5. Beniston M (2004) Climatic Change and its Impacts. An Overview Focusing on Switzerland. Kluwer Academic Publishers: Dordrecht/The Netherlands and Boston/USA (now Springer Publishers).

6. Xu C-Y, Wide'n E, Halldin S (2005) Modelling hydrological consequences of climate change - progress and challenges. Adv Atmos Sci 22 (6): 789–797.

7. Soncini A, Bocchiola D (2011) Assessment of future snowfall regimes within the Italian Alps using general circulation models. Cold Reg Sci Technol 68(3): 113–123.

8. Diolaiuti GA, Maragno D, D'Agata C, Smiraglia C, Bocchiola D (2011) Glacier retreat and climate change: Documenting the last 50 years of Alpine glacier history from area and geometry changes of Dosdè Piazzi glaciers (Lombardy Alps, Italy). Prog Phys Geog 35(2): 161–182.

9. Ficklin DL, Stewart IT, Maurer EP (2013) Climate Change Impacts on Streamflow and Subbasin-Scale Hydrology in the Upper Colorado River Basin. PLoS ONE 8(8): e71297. doi:10.1371/journal.pone.0071297.

10. Jiang T, Chen YD, Xu C, Chen X, Chen X, et al. (2007) Comparison of hydrological impacts of climate change simulated by six hydrological models in the Dongjiang Basin, South China. J Hydrol 336: 316–333.

11. Verbunt M, Gurtz J, Jasper K, Lang H, Warmerdam P, et al. (2003) The hydrological role of snow and glaciers in alpine river basins and their distributed modeling. J Hydrol 282; 36–55.

12. Null SE, Viers JH, Mount JF (2010) Hydrologic Response and Watershed Sensitivity to Climate Warming in California's Sierra Nevada. PLoS ONE 5(4): e9932. doi:10.1371/journal.pone.0009932.

13. Beniston M, Uhlmann U, Goyette S, Lopez-Moreno JI (2011) Will snow-abundant winters still exist in the Swiss Alps in an enhanced greenhouse climate? Int J Climatol 31: 1257–1263.

14. Gobiet A, Kotlarski S, Beniston M, Heinrich G, Rajczak J, et al. (2014) 21st century climate change in the European Alps–A review. Sci Total Environ 493(0): 1138–1151, doi:http://dx.doi.org/10.1016/j.scitotenv.2013.07.050.

15. Rabuffetti D, Ravazzani G, Corbari C, Mancini M (2008) Verification of operational Quantitative Discharge Forecast (QDF) for a regional warning system – the AMPHORE case studies in the upper Po River. Nat Hazard Earth Sys 8: 161–173.

16. Corbari C, Ravazzani G, Martinelli J, Mancini M (2009) Elevation based correction of snow coverage retrieved from satellite images to improve model calibration. Hydrol Earth Syst Sc 13(5): 639–649.

17. Viviroli D, Zappa M, Schwanbeck J, Gurtz J, Weingartner R (2009) Continuous simulation for flood estimation in ungauged mesoscale catchments of Switzerland – Part I: Modelling framework and calibration results. J Hydrol 377: 191–207.

18. Corbari C, Ravazzani G, Mancini M (2011) A distributed thermodynamic model for energy and mass balance computation: FEST-EWB. Hydrol Process 25(9): 1443–1452.

19. Montaldo N, Albertson JD (2001) On The Use Of The Force-Restore SVAT Model Formulation For Stratified Soils. J Hydrometeorol 2(6): 571–578.

20. Senatore A, Mendicino G, Smiatek G, Kunstmann H (2011) Regional climate change projections and hydrological impact analysis for a Mediterranean basin in Southern Italy. J Hydrol 399: 70–92.

21. Montaldo N, Mancini M, Rosso R (2004) Flood hydrograph attenuation induced by a reservoir system: analysis with a distributed rainfall-runoff model. Hydrol Process 18 (3): 545–563.

22. Regione Piemonte (1997) DTM 1/10000. *Servizio Cartografico (Cartographic Service)*: Torino (Italy).

23. CEC (2000) CORINE land cover. Technical guide, Commission of the European Communities, Luxembourg.

24. Bacchi B, Ranzi R (2003) Hydrological and meteorological aspects of floods in the Alps: an overview. Hydrol Earth Syst Sc 7(6): 784–798.

25. Montaldo N, Ravazzani G, Mancini M (2007) On the prediction of the Toce alpine basin floods with distributed hydrologic models. Hydrol Process 21: 608–621.

26. Pianosi F, Ravazzani G (2010) Assessing rainfall-runoff models for the management of Lake Verbano. Hydrol Process 24(22): 3195–3205.

27. Corbari C, Sobrino JA, Mancini M, Hidalgo V (2010) Land surface temperature representativeness in a heterogeneous area through a distributed energy-water balance model and remote sensing data. Hydrol Earth Syst Sc 14: 2141–2151.

28. Ravazzani G, Mancini M, Giudici I, Amadio P (2007) Effects of soil moisture parameterization on a real- time flood forecasting system based on rainfall thresholds. IAHS Publ. 313: 407–416.

29. Ravazzani G, Mancini M, Meroni C (2009) Design hydrograph and routing scheme for flood mapping in a dense urban area. Urban Water J 6(3): 221–231.

30. Ravazzani G, Rametta D, Mancini M (2011) Macroscopic Cellular Automata for groundwater modelling: a first approach. Environ Modell Softw 26(5): 634–643.

31. Ravazzani G, Gianoli P, Meucci S, Mancini M (2012b) Indirect estimation of design flood in urbanized river basins using a distributed hydrological model. J Hydrol Eng 19(1): 235–242.

32. Ceppi A, Ravazzani G, Salandin A, Rabuffetti D, Montani A, et al. (2013) Effects of temperature on flood forecasting: analysis of an operative case study in Alpine basins. Nat Hazard Earth Sys 13(4): 1051–1062.

33. Gaudard L, Romerio F, Dalla Valle F, Gorret R, Maran S, et al. (2013) Climate change impacts on hydropower in the Swiss and Italian Alps. Sci Total Environ, in press, doi: 10.1016/j.scitotenv.2013.10.012.

34. Ravazzani G (2013) MOSAICO, a library for raster based hydrological applications. Comput Geosci 51: 1–6.

35. Allen RG, Pereira LS, Raes D, Smith M (1998) Crop evapotranspiration – guidelines for computing crop water requirements – FAO Irrigation and Drainage Paper 56. FAO.

36. D'Urso G, Menenti M (1995) Mapping crop coefficients in irrigated areas from Landsat TM images, in Paris Europto, (Ed.) European Symposium on Satellite Remote Sensing II, SPIE, Intern Soc Optical Engineering vol. 2585, Bellingham, USA, 41–47.

37. Corbari C, Ravazzani G, Galvagno M, Cremonese E, Mancini M (2014) Assessing crop coefficient for natural vegetated area using satellite data and eddy covariance stations. J Hydrol Eng, submitted.

38. Ravazzani G, Corbari C, Morella S, Gianoli P, Mancini M (2012a) Modified Hargreaves-Samani equation for the assessment of reference evapotranspiration in Alpine river basins. J Irrig Drain Eng 138(7): 592–599.

39. Hargreaves G H (1994) Defining and using reference evapotranspiration. J Irrig Drain Eng 120(6): 1132–1139.

40. Jacobs AFG, Heusinlveld BG, Holtslag AAM (2008) Towards closing the energy surface budget of a mid-latitude grassland. Boundary Layer Meteorol 126: 125–136.

41. Meyers TP, Hollinger SE (2004) An assessment of storage terms in the surface energy balance of maize and soybean. Agr Forest Meteorol 125: 105–115.

42. Boscarello L, Ravazzani G, Rabuffetti D (2014) Integrating glaciers dynamics raster based modelling in large catchments hydrological balance: the Rhone case study. Hydrol Process 28(3): 401–1560. doi: 10.1002/hyp.9588.

43. Pellegrini M (2011) Accuracy of MODIS snow cover images and calibration of hydrological model in alpine river basins, Politecnico di Milano, Milan, Master thesis.

44. Nash JE, Sutcliffe JV (1970) River flow forecasting through the conceptual models, Part 1: A discussion of principles. J Hydrol 10 (3): 282–290.

45. Jacob D (2001) A note to the simulation of the annual and inter-annual variability of the water budget over the Baltic Sea drainage basin. Meteorol Atmos Phys 77: 61–73.

46. Pal JS, Giorgi F, Bi X, Elguindi N, Solmon F, et al. (2007) Regional climate modeling for the developing world: The ICTP RegCM3 and RegCNET. Bull Am Met Soc 88: 1395–1409.

47. Roeckner E, Baeuml G, Bonaventura L, Brokopf R, Esch M, et al. (2003) The Atmospheric General Circulation Model ECHAM5. Part 1: Model Description, Report 349, Max Planck Institute for Meteorology (MPI), Hamburg.

48. Nakicenovic N, Alcamo J, Davis G, de Vries B, Fenhann J, et al. (2000) IPCC Special Report on Emissions Scenarios, Cambridge University Press, Cambridge, United Kingdom and New York, NY, USA.

49. Heinrich G, Gobiet A, Prein AF (2011) Uncertainty of Regional Climate Simulations in the Alpine Region. EGC Report to the EU Nr. 01/2011, 59 pp, Wegener Center, University of Graz, Graz, Austria.

50. Dettinger MD, Cayan DR, Meyer MK, Jeton AE (2004) Simulated hydrologic responses to climate variations and change in the Merced, Carson, and American river basins, Sierra Nevada, California, 1900–2099. Climatic Change 62: 283–317.

51. Wood AW, Leung LR, Sridhar V, Lettenmaier DP (2004) Hydrologic Implications of Dynamical and Statistical Approaches to Downscale Climate Model Outputs. Climatic Change 62: 189–216.

52. Dobler A, Ahrens B (2008) Precipitation by a regional climate model and bias correction in Europe and South Asia. Meteorologische Zeitschrift 17: 499–509.

53. Piani C, Haerter JO, Coppola E (2010) Statistical bias correction for daily precipitation in regional climate models over Europe. Theor Appl Climatol 99: 187–192, doi: 10.1007/s00704-009-0134-9.

54. Themeßl MJ, Gobiet A, Heinrich G (2012) Empirical-statistical downscaling and error correction of regional climate models and its impact on the climate change signal. Climatic Change 112(2): 449–468. doi: 10.1007/s10584-011-0224-4.

55. Amengual A, Homar V, Romero R, Alonso S, Ramis C (2012) A statistical adjustment of regional climate model outputs to local scales: application to Platja de Palma, Spain. J Clim 25(3): 939–957.

56. Déqué M (2007) Frequency of precipitation and temperature extremes over France in an anthropogenic scenario: model results and statistical correction according to observed values. Glob Planet Chang 57: 16–26.

57. Boé J, Terray L, Habets F, Martin E (2007) Statistical and dynamical downscaling of the Seine basin climate for hydro-meteorological studies. Int J Climatol 27: 1643–1655.

58. Wilks DS (1995) Statistical Methods in Atmospheric Science, Volume 59 of International Geophysics Series. Academic Press: San Diego, London.

59. Themeßl M, Gobiet A, Leuprecht A (2011) Empirical-statistical downscaling and error correction of daily precipitation from regional climate models. Int J Climatol 31(10): 1530–1544. doi:10.1002/joc.2168.

60. Wilcke RA, Mendlik T, Gobiet A (2013) Performance and Physical Consistency of Multi-Variable Downscaling and Error-Correction of Regional Climate Models. Climatic Change 120:871–887.

61. Maraun D (2012) Nonstationarities of regional climate model biases in European seasonal mean temperature and precipitation sums. Geophys Res Lett 39: L06706. doi:10.1029/2012GL051210.

62. Christensen JH, Hewitson B, Busuioc A, Chen A, Gao A, et al. (2007) Regional climate projections. In: climate change 2007: the physical science basis. Contribution of Working Group I to the Fourth Assessment Report of the Intergovernmental Panel on Climate Change. Cambridge University Press, Cambridge, United Kingdom and New York, NY, USA.